http://dx.doi.org/10.5516/NET.08.2012.003

EXPERIMENTAL ANALYSES OF SPALLATION NEUTRONS GENERATED BY 100 MEV PROTONS AT THE KYOTO UNIVERSITY CRITICAL ASSEMBLY

CHEOL HO PYEON[1*], TETSUSHI AZUMA[2], YUKI TAKEMOTO[2], TAKAHIRO YAGI[1], and TSUYOSHI MISAWA[1]

[1]Nuclear Engineering Science Division, Research Reactor Institute, Kyoto University
Asashiro-nishi, Kumatori-cho, Sennan-gun, Osaka 590-0494, Japan
[2]Department of Fundamental Energy Science, Graduate School of Energy Science, Kyoto University
Yoshida-honmachi, Sakyo-ku, Kyoto 606-8501, Japan
[*]Corresponding author. E-mail : pyeon@rri.kyoto-u.ac.jp

Received January 13, 2012
Accepted for Publication April 30, 2012

Neutron spectrum analyses of spallation neutrons are conducted in the accelerator-driven system (ADS) facility at the Kyoto University Critical Assembly (KUCA). High-energy protons (100 MeV) obtained from the fixed field alternating gradient accelerator are injected onto a tungsten target, whereby the spallation neutrons are generated. For neutronic characteristics of spallation neutrons, the reaction rates and the continuous energy distribution of spallation neutrons are measured by the foil activation method and by an organic liquid scintillator, respectively. Numerical calculations are executed by MCNPX with JENDL/HE-2007 and ENDF/B-VI libraries to evaluate the reaction rates of activation foils (bismuth and indium) set at the target and the continuous energy distribution of spallation neutrons set in front of the target. For the reaction rates by the foil activation method, the C/E values between the experiments and the calculations are found around a relative difference of 10%, except for some reactions. For continuous energy distribution by the organic liquid scintillator, the spallation neutrons are observed up to 45 MeV. From these results, the neutron spectrum information on the spallation neutrons generated at the target are attained successfully in injecting 100 MeV protons onto the tungsten target.

KEYWORDS : ADS; KUCA; Spallation Neutrons; High-energy Protons; Reaction rates; Continuous Energy Distribution

1. INTRODUCTION

The Kyoto University Research Reactor Institute (KURRI) has engaged in innovative project of research and development of an accelerator-driven system (ADS) at the Kyoto University Critical Assembly (KUCA)[1]-[9] and an external neutron source. The main objective of the project is to develop a next-generation neutron source with the use of the ADS with high-energy protons obtained from the fixed field alternating gradient (FFAG) accelerator,[10]-[12] instead of the conventional research reactor (the Kyoto University Research Reactor: KUR; 5 MW) at KURRI. The basic concept of ADS was originally proposed as an energy amplifier system[13] that couples with a high-power accelerator and a thorium sustainable system. Another possible function of ADS was resolving the issue of nuclear transmutation of radioactive materials, including minor actinides and long-lived fission products. The current research activities on ADS involve mainly experimental feasibility studies with the use of critical assemblies and test facilities: MASURCA,[14]-[16] YALINA-booster and -thermal,[17]-[19] VENUS-1,[20] GUINEVERE[21] and KUCA.

In the ADS facility, a study on target design was requisite experimentally and numerically for examining the characteristics of spallation neutrons generated by injecting the high-energy protons before reactor physics experiments on feasibility studies of ADS. Especially dimensions of the target (size and thickness) needed to be investigated, before the actual injection of high-energy protons, because they are expected to vary in accordance with the spot and the energy of protons. The main characteristics of spallation neutrons analyzed experimentally and numerically at another irradiation facility[22] have contributed notably to the present study. On the basis of those valuable results, the present experimental study of spallation neutrons generated at the tungsten target was conducted, focusing on the neutron spectrum (reaction rates and continuous energy distribution of neutrons) at the location of the target. Special

attention was paid to the reaction rates (neutron yield and profile) with the use of bismuth (Bi) and indium (In) activation foils, and to the continuous energy distribution of neutrons using organic liquid scintillator. These experiments on continuous energy distribution of neutrons were emphasized to be carried out near the location of the target, whereas neutron spectrum measurements are usually conducted by the time of flight method at a location far from the neutron source. Further, the neutron spectrum measurement was considered difficult near the location of the target, because the accuracy of neutron detection is dependent on two factors: the distance and the time of flight of neutrons.

The neutron spectrum was considered an important parameter for recognizing information on neutron energy at the target; as a result, the experimental analyses at the target could significantly affect the neutronic characteristics of the core by numerical analyses in the feasibility study on ADS. Also, the neutron spectrum evaluated by reliable methodologies could contribute to accurate prediction of reactor physics parameters in the core through numerical simulations of desired precision. The objective of this study was to analyze experimentally the neutron spectrum of spallation neutrons generated by 100 MeV protons at the location of the target in the ADS facility, before the actual operation of ADS and the improvement of numerical simulations. The neutron spectrum experiments with 100 MeV protons generated by the FFAG accelerator are shown in Sec. 2 and include descriptions of the experimental settings. The results of experimental and numerical analyses by the Monte Carlo calculation code combined with nuclear data libraries are presented in Sec. 3 and the conclusions are summarized in Sec. 4.

2. EXPERIMENTAL SETTINGS

2.1 High-Energy Protons

High-energy protons were generated by the FFAG accelerator under the following parameters: 100 MeV energy; 30 pA intensity; 30 Hz repetition rate; 200 ns beam width. On the downstream of the FFAG beam line, the tungsten was set at the location of the original target (80 mm diameter and 10 mm thick); the thickness was determined on the basis of previous experimental and numerical analyses[22] for the injection of high-energy proton beams onto the tungsten target. For the proton beam configuration modeled by numerical simulations, the size of the proton beam spot was requisite experimentally and precisely, when 100 MeV protons were injected onto the tungsten target where the spallation neutrons are generated. The Gafchromic film,[23] which is very sensitive to the charged particles, was then used to evaluate the size of the proton beam spot injected onto the tungsten target, since a graphic image on the film is acquired quickly after the irradiation of charged particles for a short time.

2.2 Spallation Neutrons

The reaction rates for threshold energy of high-energy neutrons and the continuous energy distribution of the spallation neutrons at the target were acquired by the foil activation method and the organic liquid scintillator, respectively. The high-energy neutrons (spallation neutrons) of threshold reactions ^{209}Bi(n, xn)$^{210-x}$Bi (n = 3, to 12) over 15 MeV have been generated by the injection of high-energy protons over 100 MeV.[22] Here, to obtain the reaction rates by high-energy neutrons at the target, ^{209}Bi was selected as an activation foil (**Table 1**) to cover threshold energies over 15 MeV, and ^{115}In was selected as a normalization factor (**Table 2**) for monitoring the spallation neutrons at the target to cover threshold reactions ^{115}In(n, n')^{115m}In over 0.32 MeV. Foil dimensions at the target were as follows: ^{209}Bi, 50 mm in diameter and 3 mm thick; ^{115}In, $10 \times 10 \times 1$ mm^3, and two foils were set around the target region as shown in **Fig. 1**(a). Additionally, nine other ^{115}In foils ($10 \times 10 \times 3$ mm^3) were placed in a circle (100 mm radius) around the target at 30 degree intervals on an acryl plate, to investigate the angular distribution of spallation neutrons as shown in Fig. 1(b). The irradiation time of ^{209}Bi and ^{115}In foils was four hours for measuring the neutron yield of spallation neutrons, and their reaction rates were measured by the high-purity germanium detector (ORTEC, GEM60P). As well as in the previous study,[3],[7],[22] the detection efficiency of the germanium detector was determined by the fitting line obtained from the energy calibration with the use of several γ-ray standard sources.

The continuous energy distribution of spallation neutrons was determined by the organic liquid scintillator (Nuclear Enterprises Ltd., NE213 Scintillator; 5" in diameter and 5" long) set directly facing the tungsten target without any reactor components as shown in **Fig. 2**(a). The measurement circulation of the organic liquid scintillator was as indicated in Fig. 2(b). The main advantage of the measurement system is that the two signals (rise time and light output of γ-ray and neutron) acquired coincidently with the use of specific equipment (Laboratory Equipment Corp., Dual MCA) readily provide a two-dimensional graphic image (rise time and light output). This system allows the rise time information on two signals to accomplish easy discrimination between γ-ray and neutron, and the signals can be converted into fluorescence signals of charged particles (recoil protons generated in reaction with neutrons).

3. EXPERIMENTAL ANALYSES

3.1 High-Energy Protons

The 10 mm thick tungsten target was determined on the basis of experimental and numerical analyses[22] from the viewpoint of the full-stop of proton beams within the tungsten target. On the other hand, the proton beam irradiation experiments were carried out to monitor the size of

Table 1. Threshold Energy, Half-life and γ-ray Energy of ^{209}Bi(n, xn) $^{210-x}$Bi Reactions (x = 3 to 12)

x	Threshold energy [MeV]	Half-life ($T_{1/2}$)	Emission γ-ray energy [keV]	x	Threshold energy [MeV]	Half-life ($T_{1/2}$)	Emission γ-ray energy [keV]
3	14.42	38.3 y	569.7 (97.8)	8	54.24	1.67 h	422.1 (83.7)
			1063.6 (74.9)				658.5 (60.6)
							961.7 (99.3)
4	22.52	6.24 d	803.1 (98.9)	9	61.69	1.77 h	786.4 (9.5)
			881.1 (66.2)				935.7 (11.3)
			1718.7 (31.8)				
5	29.62	15.31 d	703.4 (31.5)	10	70.89	36.45 min	419.7 (91.3)
			1763.4 (32.5)				462.3 (98.3)
							1026.4 (100.0)
6	38.13	11.22 h	374.8 (81.8)	11	78.47	27.12 min	425.3 (22.0)
			899.2 (98.5)				560.1 (22.0)
			983.9 (59.1)				
7	45.37	11.76 h	820.2 (29.6)	12	87.94	11.85 min	562.4 (79.0)
			825.2 (14.6)				1063.4 (100.0)
			1847.3 (11.4)				

( ): Emission rate [%]

Table 2. Threshold Energy, Half-life and γ-ray Energy of ^{115}In (n, n')^{115m}In Reactions

Threshold energy [MeV]	Half-life ($T_{1/2}$)	Emission γ-ray energy [keV]
0.32	4.486 h	336.0 (45.9)

( ): Emission rate [%]

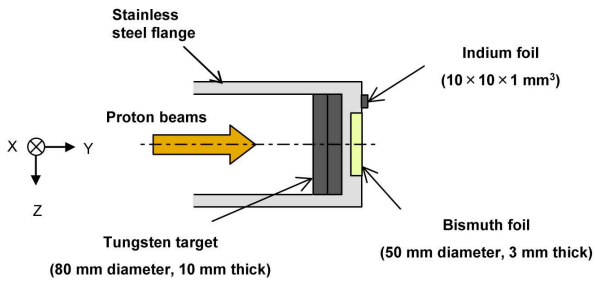

Fig. 1(a). Experimental Setting of Activation Foils (Bi and In) for Measuring the Reaction Rates at the Target Position

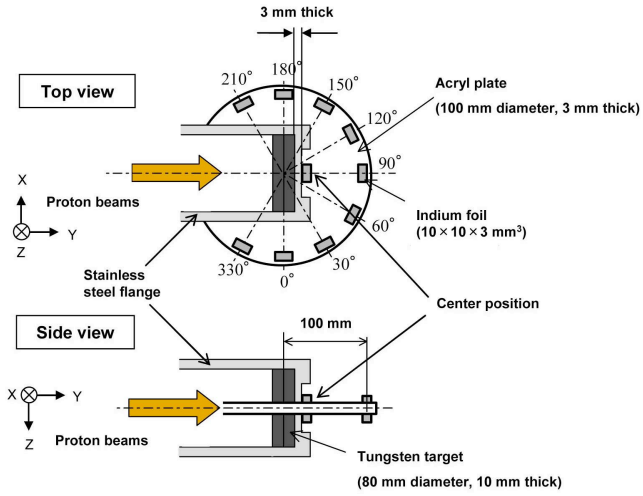

Fig. 1(b). Experimental Setting of Tungsten Target for Angular Distribution of Spallation Neutrons

the proton beam spot with the use of Gafchromic film, which is highly-sensitive to charged particles. The Gafcromic film was irradiated for two min and set on the surface (downstream beam) outside the stainless steel flange (Fig. 1) without the tungsten target, although the influence of the stainless steel flange was slightly affected to the proton beam profile. It demonstrated that the proton strength was distributed by the downstream beams (**Fig. 3**(a)), with a relative distribution within an approximately 40 mm diameter spot (Fig. 3(b)). The experimental result of the Gafchro-

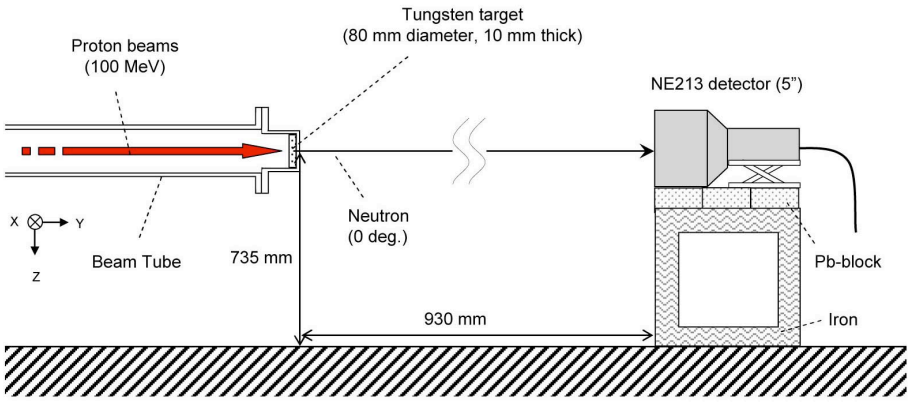

Fig. 2(a). Experimental Setting of the Organic Liquid Scintillator (NE213)

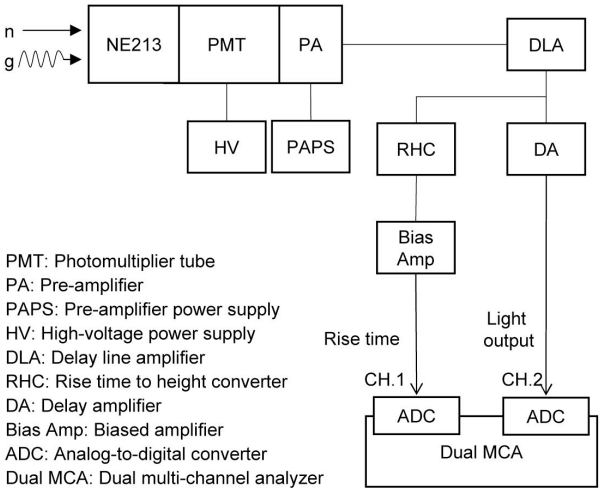

Fig. 2(b). Measurement Circulation of the Organic Liquid Scintillator (NE213)

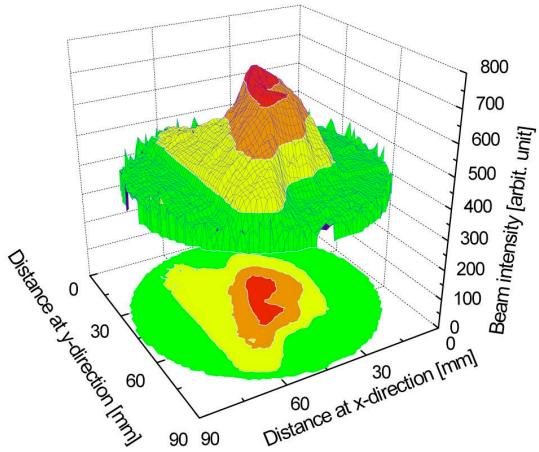

Fig. 3(b). Scanning Relative Result of Proton Strength Distribution in Fig. 3(a) of 100 MeV Protons at the Downstream Beam Without the Tungsten Target

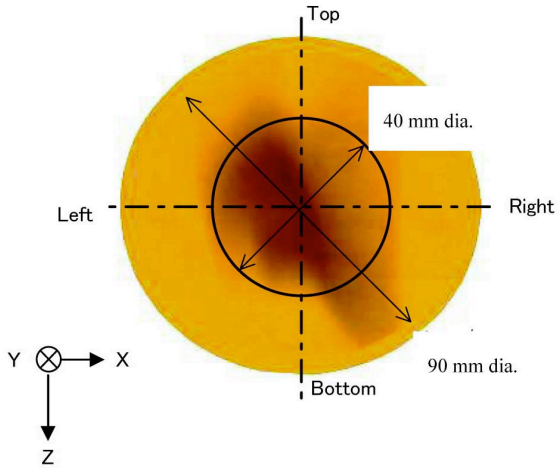

Fig. 3(a). Measured Result (Gafchromic Film) of Proton Strength Distribution of 100 MeV Protons at Upstream Beam of the Tungsten Target

mic film was very useful for modeling the size of the proton beam spot in numerical simulations, therefore, the irradiation experiments were important for evaluating the size of the proton beam spot for which the tungsten target (80 mm in diameter) was considered sufficient to cover.

3.2 Reaction Rates

The experimental results of the reaction rates were obtained by measuring total counts of the peak energy of γ-ray emissions. The saturation activity D_∞ [1/s], which is proportional to the reaction rate RR [1/s/cm^3], taking into consideration of the weight M [g] of each foil and the density ρ [g/cm^3], was calculated using the following equations:

$$D_\infty = \frac{\lambda T_c C(1+\alpha)}{\varepsilon N_\gamma \left(1-e^{-\lambda T_i}\right) e^{-\lambda T_w} \left(1-e^{-\lambda T_c}\right)} \quad , \tag{1}$$

$$RR = D_\infty \cdot \frac{\rho}{M} = \frac{\lambda T_c C(1+\alpha)\rho}{\varepsilon N_\gamma \left(1-e^{-\lambda T_i}\right) e^{-\lambda T_w} \left(1-e^{-\lambda T_c}\right) \cdot M} \quad , \tag{2}$$

where λ indicates the decay constant, T_c the measurement counting time, C the counting rate, α the internal conversion coefficient, ε the detection efficiency, N_γ the γ-ray emission rate, T_i the irradiation time, and T_w the waiting time until the start of the measurement after the irradiation. Finally, the reaction rate RR in Eq. (2) was obtained from the saturation activity D_∞ in Eq. (1).

No value for the 100 MeV proton irradiation was observed in 3n, 9n through 12n reactions of ^{209}Bi(n, xn)$^{210-x}$Bi (x = 3 to 12), since little activation was caused by insufficient irradiation with the low proton beam intensity of 30 pA and the long half-life (38.3 y) of 3n reactions. The MCNPX[24] calculations with JENDL/HE-2007[25]-[26] for nuclear data and ENDF/B-VI[27] for cross sections of Bi were executed by a total number of 2×10^8 histories within a statistical error of 1% to obtain the reaction rates of the irradiated ^{209}Bi foil. The spot size 40 mm diameter of proton beams was modeled in the MCNPX calculations on the basis of the experimental results in the Gafchromic film presented in Sec. 3-1. For the irradiation experiments of the ^{209}Bi foil, a comparison (**Table 3**) between the experimental and the numerical values showed agreement around a relative difference of 10% in the C/E (calculation/experiment) values, excluding the ^{209}Bi(n, 8n)^{202}Bi reaction. Here, from the results of the ^{209}Bi foil irradiation, the high-energy neutrons up to 50 MeV generated by ^{209}Bi(n, xn)$^{210-x}$Bi reactions were confirmed to have been bombarded by the injection of 100 MeV protons.

The measured results of the ^{115}In reaction rates for the angular are listed in **Table 4**. The highest reaction rate was observed at the center of the tungsten target shown in Table 4, and the angular distribution (**Fig. 4**(a) and Table 4) of reaction rates appeared slightly polarized in the upper direction, when all reaction rates were normalized by that at position 210 degrees, which was the largest along the angular. The reaction rate at 210 degrees was larger than at other positions, whereas the effect of the acryl plate was considered insufficient in the measured reaction rates along the angular. Next, to investigate the effect of acryl plate on measured reaction rates, numerical simulations were executed with the use of MCNPX and JENDL/HE-2007 with (w/) and without (w/o) the acryl plates. A comparison of the results (Fig. 4(b)) in the presence or absence of acryl

Table 3. C/E Values between Measured and Calculated Reaction Rates of ^{209}Bi(n, xn)$^{210-x}$Bi Reactions (x = 4 to 8) for 100 MeV Proton Beams

Reaction	C/E value
^{209}Bi(n, 4n) ^{206}Bi	1.00
^{209}Bi(n, 5n) ^{205}Bi	0.94 ± 0.01
^{209}Bi(n, 6n) ^{204}Bi	0.88 ± 0.01
^{209}Bi(n, 7n) ^{203}Bi	0.95 ± 0.02
^{209}Bi(n, 8n) ^{202}Bi	1.65 ± 0.03

Table 4. Measured Results of Indium Reaction Rates for the Angular

Position [Degree]	Measured reaction rate [1/s/cm^3]
Center	11216 ± 96
0	162 ± 5
30	229 ± 6
60	254 ± 8
90	297 ± 9
120	311 ± 10
150	343 ± 11
180	269 ± 8
210	448 ± 14
330	331 ± 10

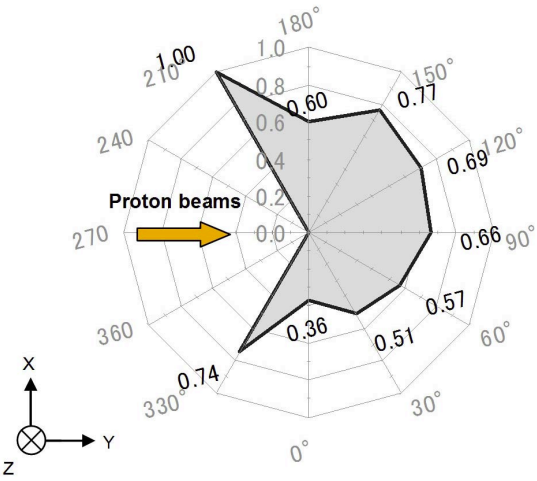

Fig. 4(a). Measured Results of Angular Distribution of Indium Reaction Rates

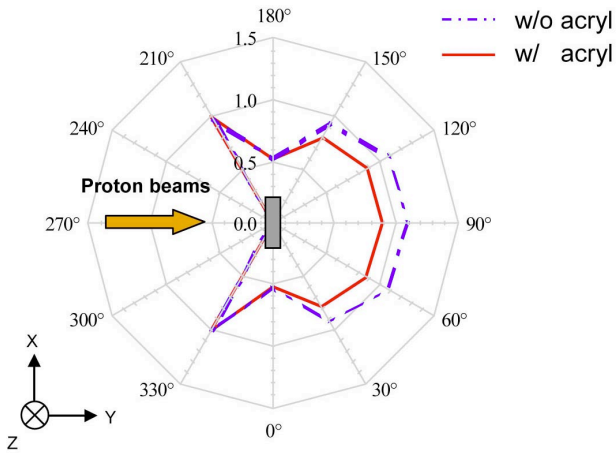

Fig. 4(b). Comparison between Calculated Results of Angular Distribution of Indium Reaction Rates with and Without the Acryl Plate

plates showed an apparent effect on the reaction rates: the high-energy neutron flux was attenuated ahead at the target and influenced by the acryl plate. Thus, the spallation neutrons were considered significantly spherical in the angular distribution through the results in numerical simulations, although their angular distribution was observed actually reversed at the target. Subsequently the neutron yield at the target was evaluated at $(9.73\pm0.12)\times10^4$ 1/s over 20 MeV and $(1.03\pm0.04)\times10^7$ 1/s over 0.32 MeV from the measured reaction rates of Bi and In foils, respectively.

3.3 Continuous Energy Distribution

The main characteristics of the measurements by the organic liquid scintillator are to acquire two signals of prompt (electrons) and delayed (protons, deuterons, or α-ray, etc.) fluorescence components and to discriminate γ-ray and neutron events caused by the two signals, respectively. Thus, the discrimination between the γ-ray and the neutron was possibly caused by the difference between their fluorescence intensities in a time-dependent manner.

A comparison between the combined (γ-ray and neutron) and the γ-ray events showed an apparent discrimination between the γ-ray and the neutron in the experimental results (**Fig. 5**) of fluorescence distributions. The γ-ray events were found to be considerably large in low-fluorescence distribution and difficult to discriminate the two events of γ-ray and neutron. The amount of fluorescence by high-energy neutrons was found to be small in high-fluorescence distribution because of very small counting rates in the high-channel region. Moreover, the spallation neutrons generated from the FFAG accelerator were considered to be a group of continuous energy neutrons with an ambiguity in maximum energy, since an edge of the recoil proton corresponding to the neutron energy was not found in the measurements by the organic liquid scintillator. Thus, the neutron energy calibration[27]-[28] of fluorescence to the light unit was conducted with the use of the results of ^{22}Na standard source (γ-ray energy; 1.274 MeV).

The neutron spectrum (**Fig. 6**) was obtained experimentally with the use of the SCINFUL-QMD code[29] for the matrix of response functions and with the UMG code[30] for the unfolding of experimental results (Fig. 5) together with the matrix by SCINFUL-QMD. As a reference of the neutron spectrum, the MCNPX calculations were executed with the use of ENDF/B-VI.6[31] for cross section data and of LA150[32] for the high-energy neutron and proton libraries. A comparison between the experiment (UMG) and the calculation (MCNPX) revealed an approximate reconstruction of the neutron spectrum in the experiment, ranging between 5 and 45 MeV neutron, although the discrepancy was observed in some energy regions. In the measurement system, the amount of fluorescence was insufficiently over 50 MeV neutron, because of detector sensitivity in relating the intensity and the energy of protons. Finally, the spallation neutrons up to 45 MeV were considered successfully detected by the organic liquid scintillator, since the discrimination between the γ-ray and the neutron was satisfactorily conducted.

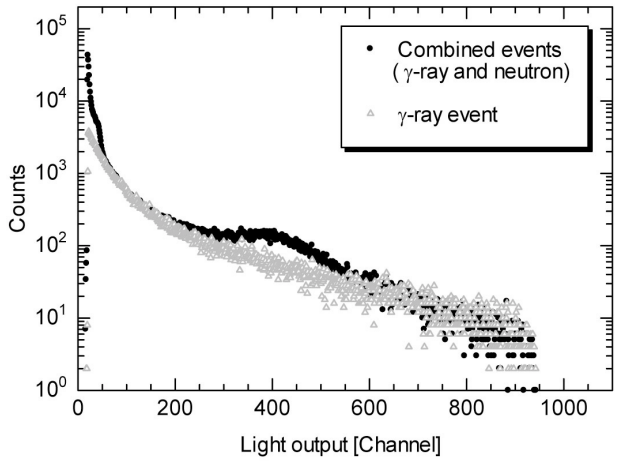

Fig. 5. Comparison between Measurement Results of Light Output from the Organic Liquid Scintillator Before and After the Discrimination of γ-ray and Neutron

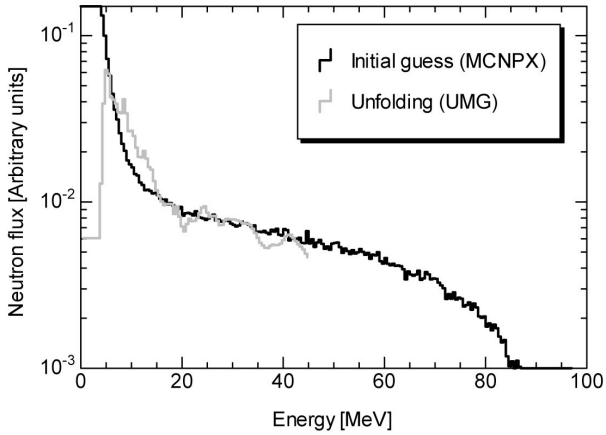

Fig. 6. Comparison between Measured (Unfolding) and Calculated (MCNPX) Results of Neutron Spectrum

4. CONCLUDING REMARKS

Neutron spectrum experiments on spallation neutrons were conducted in the ADS facility at KUCA to investigate the neutronic characteristics of spallation neutrons generated at the target. The reaction rates and the continuous energy distribution of spallation neutrons were measured by the foil activation method and by the organic liquid scintillator, respectively. For the reaction rate experiments of ^{209}Bi foil, the C/E values between the experiments and the calculations (MCNPX and ENDF/B-VI) were found well within the relative difference of 10% (^{209}Bi(n, xn)$^{210-x}$Bi; x = 4 to 7), except for some reactions (x = 8). For continuous energy distribution experiments, the spallation neutrons were observed up to 45 MeV with the use of the organic liquid

scintillator and the numerical simulations (MCNPX with JENDL/HE-2007 and ENDF/B-VI.6). From these results, the neutron spectrum information (the reaction rates and the continuous energy distribution) on the spallation neutrons generated at the tungsten target was attained successfully with the combined use of the foil activation method and the organic liquid scintillator, respectively, in the injection of 100 MeV protons obtained from the FFAG accelerator onto the tungsten target.

ACKNOWLEDGEMENTS

The authors are grateful to all the technical staff at KUCA and to the FFAG accelerator group for their assistance during the experiments.

REFERENCES

[1] C. H. Pyeon, Y. Hirano, T. Misawa *et al*., "Preliminary Experiments on Accelerator-Driven Subcritical Reactor with Pulsed Neutron Generator in Kyoto University Critical Assembly," *J. Nucl. Sci. Technol*., **44**, 1368-1378 (2007).

[2] C. H. Pyeon, M. Hervault, T. Misawa *et al*., "Static and Kinetic Experiments on Accelerator-Driven System in Kyoto University Critical Assembly," *J. Nucl. Sci. Technol*., **45**, 1171-1182 (2008).

[3] C. H. Pyeon, H. Shiga, T. Misawa *et al*., "Reaction Rate Analyses for an Accelerator-Driven System with 14 MeV Neutrons in the Kyoto University Critical Assembly," *J. Nucl. Sci. Technol*., **46**, 965-972 (2009).

[4] H. Taninaka, K. Hashimoto, C. H. Pyeon *et al*., "Determination of Lambda-Mode Eigenvalue Separation of a Thermal Accelerator-Driven System from Pulsed Neutron Experiment," *J. Nucl. Sci. Technol*., **47**, 376-383 (2010).

[5] H. Taninaka, K. Hashimoto, C. H. Pyeon *et al*., "Determination of Subcritical Reactivity of a Thermal Accelerator-Driven System from Beam Trip and Restart Experiment," *J. Nucl. Sci. Technol*., **48**, 873-879 (2011).

[6] H. Taninaka, A. Miyoshi, K. Hashimoto *et al*., "Feynman-a Analysis for a Thermal Subcritical Reactor System Driven by an Unstable 14MeV-Neutron Source," *J. Nucl. Sci. Technol*., **48**, 1272-1280 (2011).

[7] C. H. Pyeon, Y. Takemoto, T. Yagi *et al*., "Accuracy of Reaction Rates in the Accelerator-Driven System with 14 MeV Neutrons at the Kyoto University Critical Assembly," *Ann. Nucl. Energy*, **40**, 229-236 (2012).

[8] C. H. Pyeon, T. Misawa, J. Y. Lim *et al*., "First Injection of Spallation Neutrons Generated by High-Energy Protons into the Kyoto University Critical Assembly," *J. Nucl. Sci. Technol*., **46**, 1091-1093 (2009).

[9] C. H. Pyeon, J. Y. Lim, Y. Takemoto *et al*., "Preliminary Study on the Thorium-Loaded Accelerator-Driven System with 100 MeV Protons at the Kyoto University Critical Assembly," *Ann. Nucl. Energy*, **38**, 2298-2302 (2011).

[10] M. Tanigaki, K. Takamiya, H. Yoshino *et al*., "Control System for the FFAG Complex at KURRI," *Nucl. Instrum. Methods A*, **612**, 354-359 (2010).

[11] T. Planche, E. Yamakawa, T. Uesugi *et al*., "Scaling FFAG Rings for Rapid Acceleration of Muon Beams," *Nucl. Instrum. Methods A*, **622**, 21-27 (2010).

[12] T. Planche, J.-B. Lagrange, E. Yamakawa *et al*., "Harmonic Number Jump Acceleration of Muon Beams in Zero-Chromatic FFAG Rings," *Nucl. Instrum. Methods A*, **632**, 7-17 (2011).

[13] C. Rubbia, "A High Gain Energy Amplifier Operated with Fast Neutrons," *AIP Conf. Proc*., **346**, 44-53 (1995); see also P*roc. Int. Conf. on Accelerator-Driven Transmutation Technologies and Application*, Las Vegas, July 25-29, (1994).

[14] R. Soule, W. Assal, P. Chaussonnet *et al*., "Neutronic Studies in Support of Accelerator-Driven Systems: The MUSE Experiments in the MASURCA Facility," *Nucl. Sci. Eng*., **148**, 124-152 (2004).

[15] M. Plaschy, C. Destouches, G. Rimpault *et al*., "Investigation of ADS-Type Heterogeneities in the MUSE4 Critical Configuration," *J. Nucl. Sci. Technol*., **42**, 779-787 (2005).

[16] J. F. Lebrat, G. Aliberti, A. D'Angelo *et al*., "Global Results from Deterministic and Stochastic Analysis of the MUSE-4 Experiments on the Neutronics of the Accelerator-Driven Systems," *Nucl. Sci. Eng*., **158**, 49-67 (2008).

[17] C. M. Persson, A. Fokau, I. Serafimovich *et al*., "Pulsed Neutron Source Measurements in the Subcritical ADS Experiment YALINA-Booster," *Ann. Nucl. Energy*, **35**, 2357-2364 (2008).

[18] Y. Gohar, G. Aliberti, I. Bolshinsky *et al*., "YALINA-Booster Subcritical Assembly Conversion," *Trans. Am. Nucl. Soc*., **101**, 39 (2009).

[19] M. Tesinsky, C. Berglöf, T. Bäck *et al*., "Comparison of Calculated and Measured Reaction Rates Obtained through Foil Activation in the Subcritical Dual Spectrum Facility YALINA-Booster," *Ann. Nucl. Energy*, **38**, 1412-1417 (2011).

[20] H. H. Xia, "The Progress of Researches on ADS in China," *ICFA Beam Dynamics Newsletter*, **49**, 72-80 (2009).

[21] W. Uyttenhove, P. Baeten, G. Van den Eynde *et al*., "The Neutronic Design of a Critical Lead Reflected Zero-Power Reference Core for On-Line Subcriticality Measurements in Accelerator-Driven Systems," *Ann. Nucl. Energy*, **38**, 1519-1526 (2011).

[22] C. H. Pyeon, H. Shiga, K. Abe *et al*., "Reaction Rate Analysis of Nuclear Spallation Reactions Generated by 150, 190 and 235 MeV Protons," *J. Nucl. Sci. Technol*., **47**, 1090-1095 (2010).

[23] International Specialty Products, http://www.gafchromic.com/

[24] J. S. Hendricks, G. W. McKinney, L. S. Waters *et al*., "MCNPX User's Manual, Version 2.5.0.," LA-UR-05-2675, Los Alamos National Laboratory (2005).

[25] T. Fukahori, "JENDL High-Energy File," *J. Nucl. Sci. Technol., suppl*., **2**, 25-30 (2002).

[26] H. Takada, K. Kosako and T. Fukahori, "Validation of JENDL High-Energy File through Analyses of Spallation Experiments at Incident Proton Energies from 0.5 to 2.83 GeV," *J. Nucl. Sci. Technol*., **46**, 589-598 (2009).

[27] V. V. Verbinski, W. R. Burrus, T. A. Love *et al*., "Calibration of an Organic Scintillator for Neutron Spectrometry," *Nucl. Instrum. Methods*, **65**, 8-25 (1968).

[28] G. Dietze and H. Klien, "Gamma-Calibration of NE-213 Scintillator Counters," *Nucl. Instrum. Methods*, **193**, 549-556 (1982).

[29] P. F. Rose, "ENDF-201, ENDF/B-VI Summary Documentation," BNL-NCS-17541, 4th Edition (1991).

[30] D. Satoh, T. Sato, N. Shingyo *et al*., "SCINFUL-QMD:

Monte Carlo Based Computer Code to Calculate Response Function and Detection Efficiency of a Liquid Organic Scintillator for Neutron Energies up to 3 GeV," JAEA-Data/Code, 2006-23 (2006).
[31] M. Reginatto, B. Wiegel, A. Zimbal *et al*., "The UMG-Code Package, Ver. 3.3," NEA-1665/03, (2004). OECD/NEA
[32] V. Mclane, ed., "ENDF-102: Data Formats and Procedures for the Evaluated Nuclear Data File ENDF-6," BNL-NCS-44945-01/04-Rev., (2001).